APPLIED MATERIALS AND TECHNOLOGY

Jamt.ejournal.unri.ac.id

Research Article

Quantum accessory for solar panels: A sustainable solution to improve energy efficiency based on the circular economy

Camila G. Sastre[1]*, Juliana de C. Izidoro[1,2], Wayner de S. Klën[1], Mariana Araújo[2], Danilo L. Costa-Silva[2]

ABSTRACT: Carbon quantum dots (CQDs) have emerged as promising spectral modifiers for photovoltaic devices due to their photoluminescent down-conversion properties. In parallel, silica-rich industrial residues represent an environmental liability but also a potential source of functional materials. This study investigated the valorization of SiO_2-rich mining residue for the production of a sodium silicate matrix incorporating CQDs as a spectral conversion overlayer for solar panels. The treated residue successfully yielded sodium silicate, and CQDs were synthesized and integrated into the matrix. Photovoltaic testing demonstrated that panels coated with industrial-derived sodium silicate exhibited an initial efficiency increase of 8.91% compared to standard panels. However, coatings containing CQDs with the residue-derived sodium silicate showed reduced performance in early-stage testing, and all samples exhibited progressive opacity after six months, indicating limited long-term stability. These findings highlight both the potential and the challenges of integrating CQD-based spectral management with mining residue valorization. While the approach demonstrates feasibility in short-term performance enhancement, material stability remains a critical barrier for practical implementation.

Keywords: *Industrial residue, Solar panels, Quantum dots, Sodium silicate, Circular economy*

1. INTRODUCTION

Industrial solid residues are generated throughout multiple stages of consumer goods manufacturing, and a significant fraction of these materials lack economically viable reuse pathways. In Brazil, mining tailings constitute a critical environmental and geotechnical concern, as they are predominantly stored in tailings dams. These facilities present inherent risks, including slope instability, structural failure, and contaminant release, potentially leading to soil degradation and surface and groundwater contamination [1]. Recurrent failures of such storage systems have underscored the limitations of conventional residue management practices and the urgent need for sustainable valorization strategies capable of reducing long-term storage dependence.

Notably, tailings from the Mariana disaster exhibit high silica content, which is particularly relevant given that SiO_2 serves as a fundamental precursor in the production of semiconductors, glass, and silicate-based materials [2,3]. Such materials are extensively employed in photovoltaic and optoelectronic applications and are produced at large industrial scale, reinforcing the technological value of silica-rich residues. Owing to its optical transparency and chemical stability, sodium silicate can function as an inorganic matrix for nanomaterial dispersion while maintaining high optical transmittance, making it suitable for photovoltaic overlayer applications. The development of novel materials derived from industrial residues aligns with the principles of the circular economy, an economic framework proposed as an alternative to the conventional linear production model. The circular economy is founded on three core principles: preserving natural capital, optimizing resource utilization in production systems, and enhancing overall system efficiency [4].

OPEN ACCESS

Affiliation

[1]Programa Cientista aprendiz, Colégio Dante Alighieri, 01420-001 São Paulo - SP, Brasill.

[2]Instituto de Pesquisas Energéticas e Nucleares – IPEN/CNEN, 05508-000 São Paulo – SP, Brasil.

***Correspondence**

Email: Camila.gsastre@gmail.com

ORCID

Camila G. Sastre: 0009-0001-1390-5277
Juliana de C. Izidoro: 0000-0002-3466-5196
Wayner de S. Klën: 0000-0002-4105-297X
Danilo L. Costa-Silva: 0000-0001-5852-637X
Mariana Araújo: 0000-0002-0519-6263

Received: February 3, 2026
Revised: February 21, 2026
Accepted: March 27, 2026

How to cite: Sastre, C., G., Izidoro, J., de C., Klën, W., de S., Araújo, M., Costa-Silva, D., L., (2026). Quantum accessory for solar panels: A sustainable solution to improve energy efficiency based on the circular economy. *Journal of Applied Materials and Technology*, 7(2), 85–93. https://doi.org/10.31258/Jamt.7.2.85-93.

In the context of the circular economy, and considering that mining residues may exhibit high silica content [2, 4], alternative valorization pathways for their disposal are increasingly being investigated, including their potential application in the photovoltaic industry. The recovery and functional use of silica-rich tailings may contribute to resource efficiency while reducing environmental liabilities associated with large-scale tailings storage.

In parallel, the accelerated depletion of non-renewable terrestrial resources, such as petroleum, coal, and natural gas, has intensified global demand for sustainable energy alternatives. Consequently, renewable energy technologies, particularly solar and wind power, have gained increasing strategic relevance [5].

Photovoltaic devices operate based on the photovoltaic effect, a solid-state physical phenomenon in which incident photons promote electrons from the valence band to the conduction band of a semiconductor material, generating electron–hole pairs. The separation and directed movement of these charge carriers under the influence of an internal electric field produce an electric current. To enhance device performance, semiconductor materials are intentionally doped with controlled impurities to create n-type regions (electron-rich) and p-type regions (hole-rich). The interface between these regions forms a p–n junction, which establishes the built-in electric field responsible for charge separation and efficient current generation [5].

However, the technology that dominates the market has an efficiency of approximately 33.0% [5], as a result, researchers have been seeking ways to reduce the cost of the product and enhance its efficiency; one promising strategy is the incorporation of nanostructured materials, such as quantum dots. These semiconductor nanocrystals exhibit three-dimensional quantum confinement of charge carriers, leading to discrete energy levels and size-dependent optical properties, with a size ranging from 1 to 10 nanometers [6]. These quantum dots have the ability to absorb and emit radiation in the visible spectrum, as well as in adjacent regions such as infrared and ultraviolet. This variation in energy is attributed to the size of the quantum dot [6].

The quantum dot operates based on the transition of electrons between the valence band and the conduction band, with a so-called forbidden band existing between them. This band varies in size according to the dimensions of the quantum dot, having an inversely proportional relationship. As the size of a quantum dot decreases, quantum confinement becomes more pronounced, leading to an increase in band gap energy and preferential absorption of higher-energy photons. Conversely, larger quantum dots exhibit smaller band gaps and absorb lower-energy radiation [7]. This size-dependent tunability enables controlled spectral management through photoluminescent down-conversion, whereby high-energy photons are re-emitted at longer wavelengths. By shifting the incident solar spectrum toward regions more effectively absorbed by photovoltaic materials, this approach has the potential to enhance overall power conversion efficiency.

Spectral conversion strategies, originally explored in dye-sensitized systems, have progressively evolved and are now considered competitive enhancement technologies in photovoltaic research [8]. Notably, only approximately 33% of the solar spectrum lies within the optimal absorption range of conventional silicon-based solar cells. A significant portion of incident radiation is lost through thermalization processes, while photons with energies below the semiconductor band gap (19%) are not absorbed. Additional recombination and optical losses account for roughly 15% of the incoming energy [8]. In this context, quantum dots function as spectral modifiers that improve the utilization of incident solar radiation. Beyond photovoltaic applications, their tunable optical properties have enabled widespread use in display and optoelectronic technologies [8].

Carbon-based quantum dots are particularly attractive due to their low toxicity, chemical stability, and compatibility with sustainable synthesis routes. Nevertheless, compared to metal-based quantum dots, carbon quantum dots generally exhibit lower photoluminescence quantum yields and more limited emission wavelength tunability due to the greater difficulty in achieving precise size control. Despite these limitations, their straightforward synthesis and the wide availability of low-cost precursor materials make them particularly suitable for the present application. Although CQD-based spectral conversion layers have been widely investigated, most strategies involve their integration within the photovoltaic device structure, frequently necessitating modification or replacement of existing panels. Comparatively, limited research has examined their use as external spectral-modifying accessories, especially when combined with residue-derived silicate matrices as a sustainable material platform. Moreover, the simultaneous assessment of photovoltaic efficiency enhancement and mining residue valorization remains underexplored. This study advances CQD-based spectral conversion by testing a non-invasive, replaceable overlayer rather than device-integrated modifications, using residue-derived sodium silicate as a transparent inorganic host material within a circular-economy approach.

2. MATERIALS AND METHODS

The methodology of this article consisted of utilizing a sample of sandy residue from a mining industry (derived from iron ore processing), also referred to in this project as raw residue (RB), and conducting physical and chemical separations in order to obtain a purer starting material, termed treated residue (RT).

The treated residue was used to synthesize sodium silicate (SS), which in turn was applied as a dispersing agent for carbon quantum dots. This methodology is summarized in Figure 1.

As can be observed in Figure 1, the developed methodology consisted of treating the residue with HCl at a concentration of 0.1 mol L-1. and subsequently, magnetic separation of this material was performed, thus obtaining a magnetic fraction and a non-magnetic fraction, referred to as treated residue (RT). The non-magnetic fraction was melted together with NaOH for the formation of sodium silicate (SS), which was then solubilized in water for subsequent application

The residue sample used in this study was provided by the mining company Samarco in the year 2017 and sent to the chemistry laboratory of Colégio Dante Alighieri.

2.1. Treatment and purification of the residue. In this manner, 200 g of sandy residue from Samarco were mixed with 1L of hydrochloric acid at a concentration of 0.1 mol.L^{-1}. The suspension was filtered and washed with distilled water. Subsequently, the solid residue was dried in an oven at 120°C for 9 hours. The second stage of purification involved the removal of iron present in the residue. In this stage, the residue was subjected to a high-field

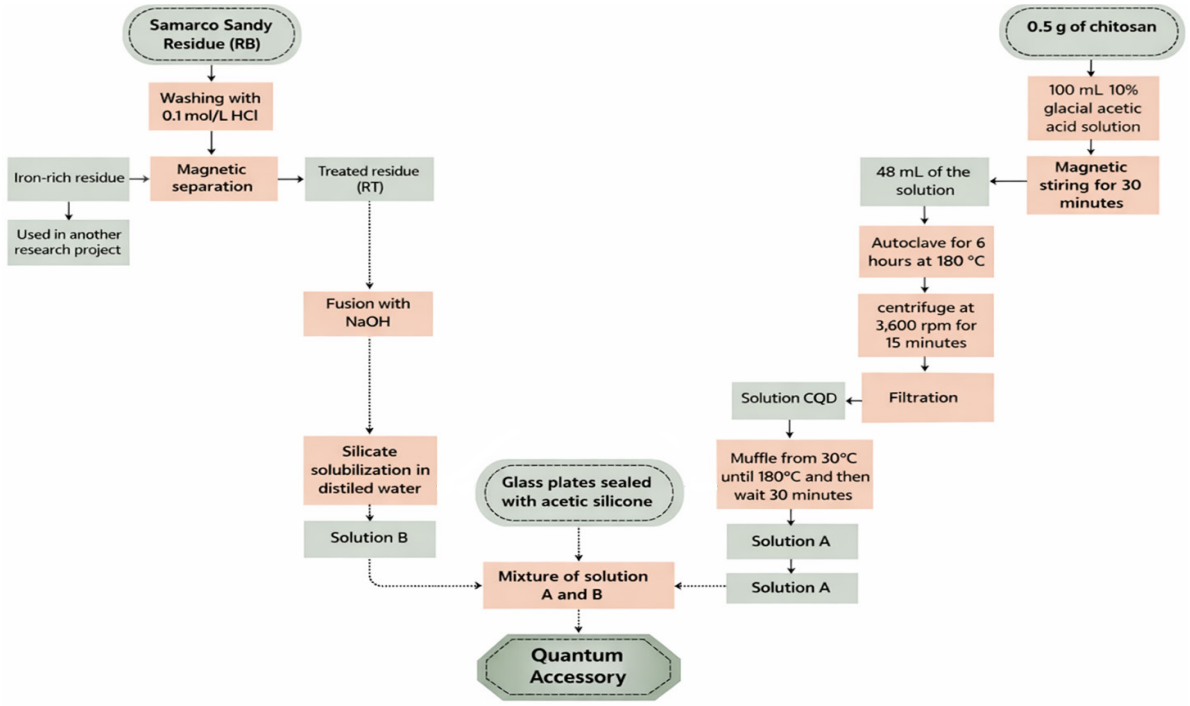

Figure 1. The diagram provides a clear and reproducible overview of the experimental procedure.

magnetic separator, from the brand Inbras, model WHC-00B, with the aim of separating the magnetic fraction from the non-magnetic fraction. This separation was conducted using a 2.5 mm grooved plate. Due to the fine particle size of the material, a wet separation method was chosen to minimize losses due to suspension. The residue was initially separated into two fractions of 250.0 g each. Subsequently, 500 mL of water was added. The material was homogenized and subjected to magnetic separation with an intensity of 1.3×104 and a current of 10.5 A. Afterwards, the magnetic fraction was removed by washing after the separator was turned off, and then both residues were subjected to a filter press at 40 bar of pressure. Finally, the residues were dried in an oven at 105°C for 17 hours and then weighed.

2.2. Obtaining sodium silicate. In The third stage of the project involved the melting of the treated residue with sodium hydroxide (NaOH) from the Synth brand. The sample was then mixed with solid NaOH and macerated in a ratio of 1:1.5. and the mixture was subjected to a fusion at 400°C for 1 hour. After the fusion, the sample was cooled to room temperature, and then 20 mL of distilled water was added. This stage was carried out based on the methodology of Rovani [9], that underwent some adaptations.

2.3. Characterization of raw residue, treated residue, and sodium silicate. The sample of raw residue (as received by the mining company, referred to in this study as RB) and the treated residue (RT) were subjected to a chemical analysis using X-ray fluorescence technique, equipment from the brand Rigaku, model Supermini 200. To determine whether the chemical compounds present in the samples were in crystalline or amorphous form, as well as to assess any changes before and after the treatment of the residue, both RB and RT samples were subjected to X-ray diffraction analysis. The equipment used was the X-ray diffractometer (DRX - Rigaku – Miniflex II) equipped with a monochromator and Cu K-α radiation, generated at 30 kV and 15 mA. The scan speed was set at $0.05°s^{-1}$ with 2θ varying between 10 and 80 degrees. The identification of crystalline phases was assisted by the Search-Match computer program.

The technique of scanning electron microscopy (SEM) was used to compare the morphology of the RB, RT, and product (sodium silicate - SS). The equipment used was the Tabletop Microscope TM3000 by Hitachi.

2.4. Synthesis of carbon quantum dots from chitosan. The methodology used for the synthesis of carbon quantum dots was adapted from the work of Gumathannavar (2026) [10]. Therefore, 0.5 g of chitosan (Sigma-Aldrich brand) was dissolved in 100 mL of a 10% glacial acetic acid solution.

The solution was kept under magnetic stirring for 30 minutes, resulting in a gel. A volume of 48 mL of the gel was transferred to a 150 mL autoclave made of stainless steel and coated with Teflon. This assembly was heated for 6 hours at 180°C. The solution was then centrifuged at a speed of 3,900 rpm for 15 minutes, and the quantum dots were subsequently filtered. A thermal treatment was then performed, during which the entire filtered volume (approximately 48 mL) was placed in a porcelain capsule. This capsule was placed in a muffle furnace, starting at an initial temperature of 30°C and ramping up to 180°C.

Once the expected temperature was reached, the timer was set to 30 minutes, then the quantum dots that were previously in solution went to the solid state. This solid was put in suspension with the addition of 8 mL of distilled water. The synthesis of carbon quantum dots (CQD) was carried out in the chemistry laboratory of Colégio Dante Alighieri. The infrared spectroscopy technique was used to verify the formation of the carbon quantum dots (CQD). The equipment used was the Nexus 870FTIR model from Thermo Nicolet and the evaluation range was from 400 to 4,000 cm^{-1}.

2.5. Manufacturing of the solar panel accessory. The fabrication of the quantum accessory was done using two glass plates with a thickness of 2 mm, in a square shape with sides of 5 cm. Sodium silicate dissolved in water at a ratio of 4 g of silicate to 6 mL of distilled water was used as a dispersing agent. This suspension was homogenized and the material then underwent a filtration step. The accessory containing quantum dots was developed in the same way as previously described, but 2 mL of the CQD solution was added. The materials were pressed between glass plates and sealed with silicone.

2.5.1. *Development of the data collection system on the solar panel.* The experimental setup consists of two study groups: a control group, containing only pure glass plates, and the experimental groups, containing the glass plates and a thin layer of the materials to be tested. Thus, a system comprising the solar panel, glass plates (control group), and glass plates containing sodium silicate with or without quantum dots (experimental groups), a lamp, and an Arduino Uno Rev 3 for power measurement was assembled in the maker laboratory of Colégio Dante Alighieri. In order to better control the variables within the experiment, a design of a 3 mm thick MDF box was created into which the plates were inserted. A hole was then made at the top of the box to fit the socket of a 200W incandescent bulb to power the solar panel. To perform the measurements of power and energy produced, an Arduino UNO microcontroller connected to an INA219 sensor (current and voltage) was used, Figure 2.

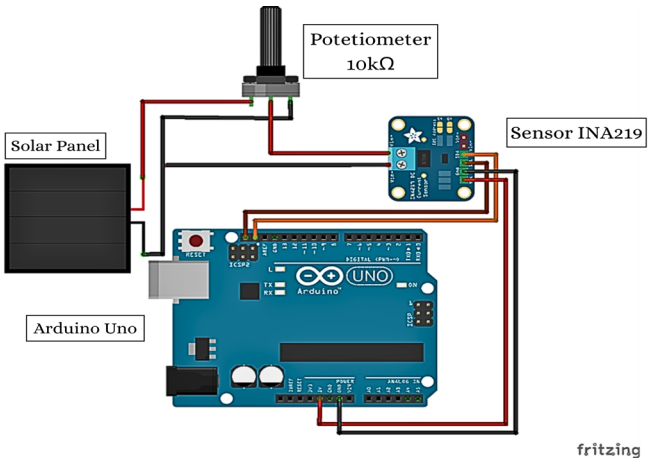

Figure 2. Connection diagram of the electrical power measurement system produced by the solar panel.

A solar panel was connected to a 10kΩ potentiometer and illuminated by an incandescent lamp. Data collection occurred over a 5-minute interval with the solar panel temperature close to 0°C. Each panel was tested separately in 4 groups. In the first group, only the value of the solar panel and two 2 mm thick glass plates were measured, with no filling between them. This plate was placed with the aim of establishing a control group regarding the expected value. In the second and fourth groups, sodium silicate plates with quantum dots (with the silicate derived from the residue) and sodium silicate plates with commercial quantum dots were tested. In the third group, sodium silicate derived from the residue without the quantum dots was tested.

2.5.2. *Data treatment and statistics.* For the treatment of the obtained data, Gaussian uncertainty propagation was used in order to obtain results that take into account the standard deviation of the measurements. The formula employed in the calculation of gain is given by Eq. (1) [11].

$$G(\mu_e,\mu_c)=\frac{\mu_e}{\mu_c}\cdot 100-100 \qquad \text{Equation 1}$$

where μ_e is the average of a set of measurements from one of the groups and μc is the average of a set of reference measurements. The final gain, in turn, will be given in percentage. In our case, the reference set was the electrical power measurements obtained by the control group. The general formula used to calculate the propagation of errors considering two variables was shown in the Eq. 2 [12].

$$\sigma_G=\sqrt{\left(\frac{\partial G}{\partial \mu_e}\sigma_{\mu e}\right)^2+\left(\frac{\partial G}{\partial \mu_c}\sigma_{\mu c}\right)^2} \qquad \text{Equation 2}$$

Calculating the partial derivatives of G with respect to μe and μc, we obtain,

$$\frac{\partial G}{\partial \mu_e}=\frac{100}{\mu_c},$$

$$\frac{\partial G}{\partial \mu_c}=-\frac{100\mu_e}{\mu_c^2}$$

Therefore, the error associated with the gain is given in the Eq. 3.

$$\sigma_G=100\sqrt{\left(\frac{\sigma_{\mu e}}{\mu_c}\right)^2+\left(\frac{\mu_e\sigma_{\mu c}}{\mu_c^2}\right)^2} \qquad \text{Equation 3}$$

With these three equations, it is possible to calculate the error associated with the experiment's gain. Additionally, it will be verified whether the datasets found in the different groups are statistically different, in order to ascertain whether we indeed have significantly different measures among the groups. To that end, a Kolmogorov-Smirnov (KS) normality test will be applied to each of the samples data set. We chose this test because each group produced a time series of electrical power measurements, totaling 149 time points collected during one continuous 5-min run per group. For these sample sizes, the KS test proves to be more robust. The KS test performs this verification through the statistic [13] in Eq. 4.

$$D_n=\sup_X\left|F_n(x)-F(x)\right| \qquad \text{Equation 4}$$

Where sup is the supremum of the set of distances, $F_n(x)$ is the value of the empirical distribution function, and $F_n(x)$ is the value of the theoretical normal function. The criterion adopted for rejecting the null hypothesis was based on the p-value provided by the test; specifically, the null hypotheses were rejected when $p < 0.05$. Subsequently, a non-parametric Friedmann rank test was applied to verify the statistical similarity among the samples. This test was chosen as it is an ideal non-parametric test for repeated measures, as in the present experiment. Finally, an additional post-hoc test was conducted. The Conover test was applied pairwise to evaluate which groups differed statistically. All of this statistical treatment was performed in the Wolfram Mathematica Student version 14.2 computing environment.

3. RESULT AND DISCUSSION

3.1. Residue treatment. As previously mentioned, the raw residue (RB) was subjected to washing with hydrochloric acid. A decrease in mass was observed at this stage, indicating that some of the impurities were solubilized in the acid, and there was also a loss of material during the filtration stage. This experiment was performed in triplicate, and the results are shown in Table 1.

Table 1. Mass of residue before and after washing with acid.

Mass of residue before washing	Mass of residue after washing	Percentage of loss
200.0g	191.2g	4.4%
200.0g	197.5g	1.2%
200.0g	198.2g	0.8%

A 500.0 g mass of the treated residue (RT) was subjected to high-intensity magnetic separation at a partner company (according to the methodology). Finally, the resulting products were weighed, with the final mass values being 405.1 g for the non-magnetic fraction and 90.8 g for the magnetic fraction. Amaral (2021) [14] determined the chemical composition of an industrial residue also supplied by Samarco S.A., which showed a high percentage of quartz and hematite, corroborating the results of this study. It is worth noting that the treatment of mining residue through acid leaching was also used in the work of Zhu (2025) [15], which used HCl to solubilize impurities and enrich the material in SiO_2, Zhu also used a magnetic separation step on an iron ore residue during its treatment.

3.2. Characterization of residue (RB and RT) and product (SS). The raw residue (RB), the treated residue (RT), as well as the sodium silicate (final product - SS), were subjected to X-ray fluorescence (XRF) analysis to verify the changes in chemical composition after the steps. The results are shown in Table 2. As shown in Table 2. it is possible to observe that after the washing procedures with HCl and magnetic separation, the iron content present in the sample decreased, thus increasing the purity of the silica (which was the initial objective of these procedures), since the yield of the next reactions involving silica would be higher.

It should be noted that the percentage of iron found in residues of this type may vary according to the mine and the specific geological characteristics of the region. In the work of Ayala-Durán (2020) [16] XRF analysis of iron mining residue by X-ray fluorescence showed 25.5% Fe; however, on Durán and Cristina study, the objective was to use that material for low-cost and environmentally compliant catalyst in Fenton processes, while in this work, the objective was to obtain the silica present in the sample.

When other types of residues are used, it is possible to verify that there is a large difference in the chemical composition results determined by XRF, as for example in Zhan's study [17] in which a residue from iron extraction was used to construct the hydraulic barrier of a landfill cover. The analysis showed a higher content of Ca_2SiO_4, approximately 33.1% in residue. However, the contents of SiO_2 were much smaller, approximately 5.7%. Furthermore, in the formation of sodium silicate, it was observed that most of the impurities identified in the raw residue and the treated residue were no longer present in the sample, in addition to a significant increase in Na_2O due to fusion with caustic soda (NaOH). The X-ray diffractograms of the RB, RT and SS samples is presented in Figure 3.

Table 2. Chemical composition of the samples determined by XRF technique (% by mass).

Components, %	RB - Raw Residue	RT - Treated Residue	SS - Sodium Silicate
SiO_2	79.30	92.20	42.40
Fe_2O_3	19.30	6.68	4.01
Al_2O_3	0.46	0.54	0.85
Cr_2O	0.15	-	0.04
MgO	0.04	0.03	-
SO_3	0.04	-	-
P_2O	0.03	0.03	-
K_2O	0.03	0.02	-
CaO	0.03	0.01	-
TiO_2	0.02	0.02	-
MnO	0.02	-	-
Na_2O	<0.01	-	52.70
Other	<0.01	<0.01	-
PF	0.5	0.41	-

As shown in Figure 3, the raw residue (RB) is mainly composed of the SiO_2 quartz phase. After treatment of the residue, the treated residue (RT) also presented the same quartz phase. Thus, it is believed that the iron present in RB was not in the crystalline phase, since it appeared in the XRF result but was not observed in the diffractogram of RB.

As can be seen in Figure 3, sodium silicate was the product formed after the fusion step with NaOH. The pattern corresponding to the Search-Match program was number 16-818, according to the database. Sodium silicate has the formula Na_2SiO_3 and was the main phase of the product. In addition, a small amount of quartz, remaining from the residue, was detected in the product.

The results found in the XRD analysis were also observed in the literature, similar XRD behavior has been reported for silica-rich iron ore tailings, where quartz (SiO_2) remains the dominant phase while acid leaching reduces impurity-related signals during purification accordingly with the work of Yongkui Li (2023) [18].

Figure 4 shows the morphology of the raw residue (RB), the treated residue (RT), and the final product after melting (sodium silicate - SS). These images were obtained using scanning electron microscopy (SEM) at 500X magnification.

As can be seen in Figure 4, the micrograph of the RB sample (1st image) has better definition and contrast than the other two images. This occurred because this sample was analyzed before the other two samples, and subsequently, the equipment underwent maintenance, altering its settings and resulting in images with lower resolutions. In any case, the images obtained were included because the scanning electron microscopy technique is complementary to the result obtained by XRD. Thus, it was possible to observe that the RB and RT samples (1st and 2nd images) are formed by

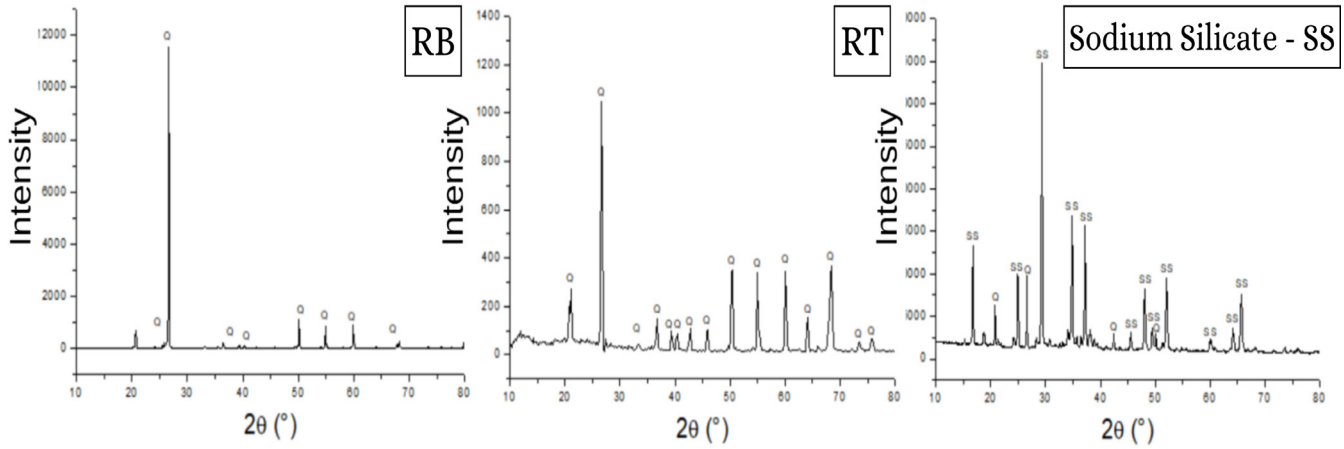

Figure 3. X-ray diffractogram of the raw residue sample (RB) treated residue sample (RT) and sodium silicate sample (SS).

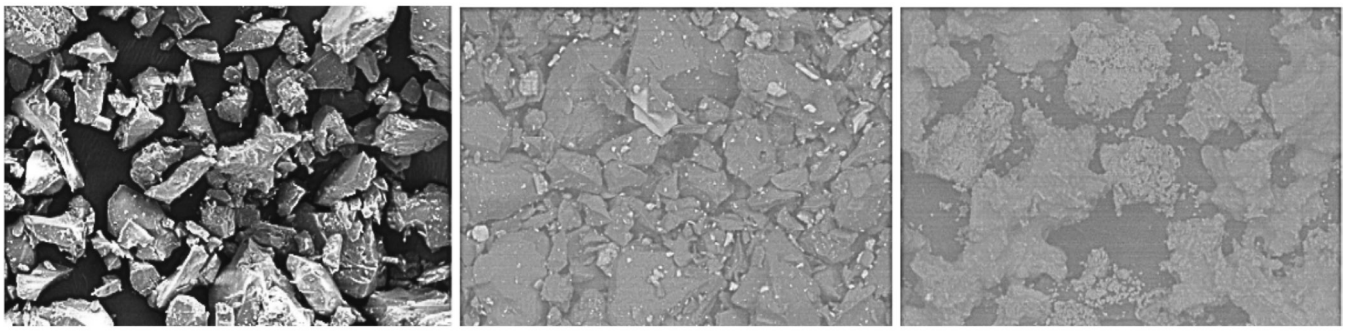

Figure 4. Micrographs of samples of raw residue, treated residue, and sodium silicate obtained by Scanning Electron Microscopy (SEM).

rigid structures of different sizes and irregular morphologies, while the SS sample has regular structures, showing that a crystalline compound was formed (as evidenced by the X-ray diffractometry technique - Figure 3).

In Gomes' work [19] a micrograph of a silica-rich residue was observed, where the sample morphology had characteristics similar to those observed in the first sample of this study, with an irregular shape. Furthermore, the aforementioned sample had a predominance of SiO_2.

3.3. Synthesis and characterization of carbon quantum dots – CQD. A small portion of the carbon quantum dots synthesized from chitosan was placed on a watch glass and subjected to an oven at 105°C for 1 hour. The product was characterized using Fourier transform infrared (FTIR) spectroscopy. The result is shown in Figure 5. The FTIR result shown in Figure 5 is consistent with the result obtained by Gumathannavar, 2026 [10] who also synthesized CQD from chitosan. Some differences in the FTIR curve may be related to the adaptation of the CQD preparation procedure, mainly related to the centrifugation step. As can be seen in the figure, the FTIR spectrum of the CQD sample showed an intense absorption band at 1,790 - 1,670 cm^{-1}, characteristic of the C=O bond originating from amide. Another band, this time wider,

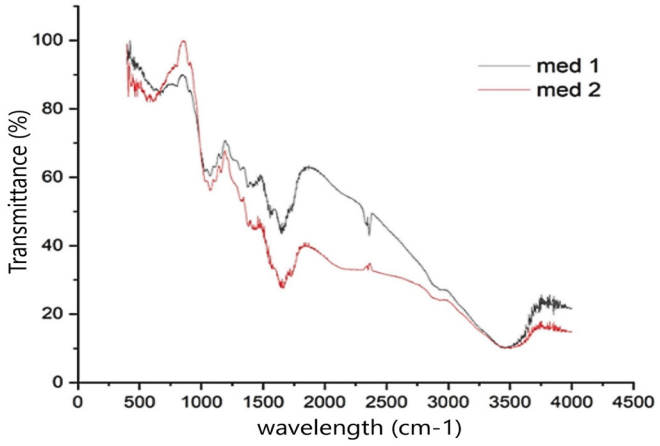

Figure 5. Spectrum of quantum dots obtained by Fourier Transform Infrared Spectrometry (FTIR).

was observed around 3500 cm^{-1}. This band corresponds to the -OH bond. Other bands were also observed at wavelengths around 1,600 cm^{-1}, 1,530 cm^{-1}, 1,360 cm^{-1} and 1,220 cm^{-1}, which correspond to the bonds C=C, N-H, C-N= and C-O [20].

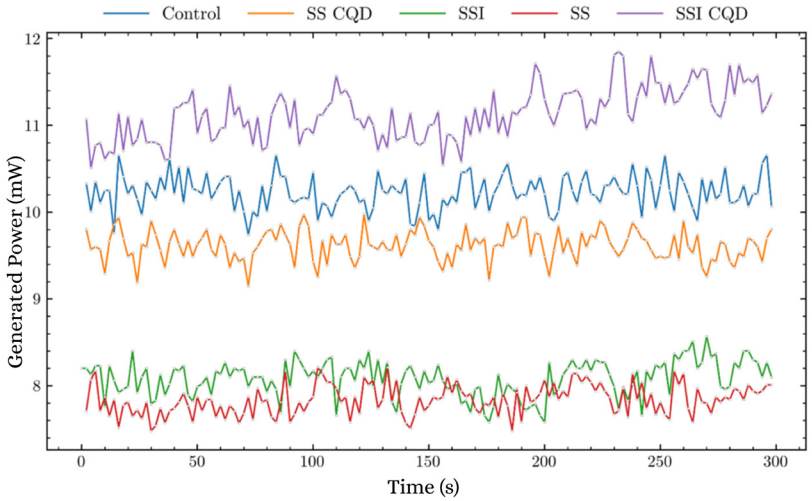

Figure 6. Power data generated by the device.

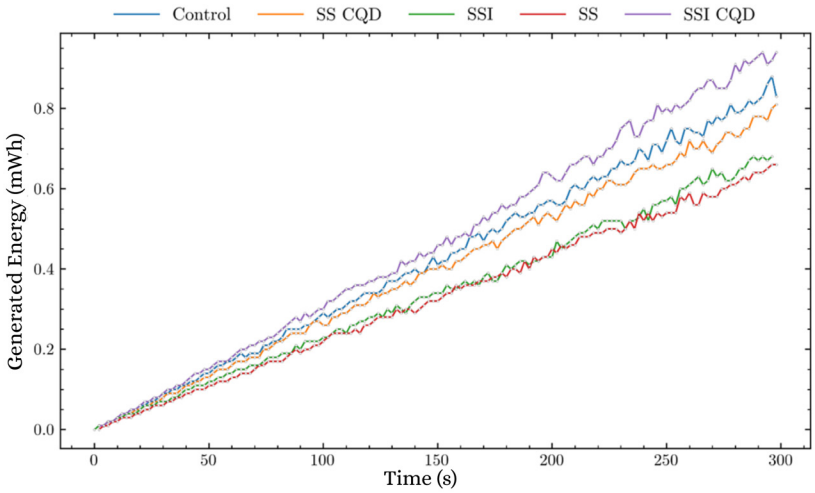

Figure 7. Energy data generated by the device.

The same result was observed in Konwar's [21] which also synthesized carbon quantum dots from chitosan. The results showed the presence of peaks in the 2,000 cm^{-1} region, as well as valleys in the regions near 1,500 cm^{-1} and 3,500 cm^{-1}.

3.4. Obtaining and characterizing the quantum accessory. The collected data yielded a graph with the aim of comparatively analyzing the results between the control group (glass only), experimental group 1 (glass and silicate residue – SS), experimental group 2 (glass, silicate residue, and quantum dots – SS CQD), experimental group 3 (glass and industrial sodium silicate – SSI), and experimental group 4 (glass, industrial sodium silicate, and quantum dots – SSI CQD). The power and energy graphs are shown in Figures 6 and 7.

As can be observed in Figures 6 and 7, the SSI-CQD group exhibited an average power output of 11.12 ± 0.29 mW, corresponding to an 8.91% increase relative to the control (10.21 ± 0.20 mW). This increase in efficiency is likely associated with the photoluminescent down-conversion mechanism of carbon quantum dots, which absorb high-energy photons and re-emit them at wavelengths more closely aligned with the spectral response of silicon photovoltaic cells. However, the performance of the accessory with industrial sodium silicate was superior to that of the silicate made from the residue. The reason for this difference may have been due to the presence of impurities that could not be removed from the residue and thus reduced optical transparency. In addition, the commercial sodium silicate and the sodium silicate from the residue had inferior results to the control group. Therefore, this suggests that sodium

Table 3. Mean and standard deviation associated with the results obtained in the solar panel efficiency experiment.

Group	Average of the results (mW)	Standard deviation (mW)
Control	10.21	0.20
SS CQD	9.63	0.17
SSI CQD	11.12	0.29
SS	7.84	0.17
SSI	8.10	0.21

Table 4. Variation in efficiency in each group of the experiment.

Group	Gain compared to the control group (%)
SS CQD	-5.68 ± 2.49
SSI CQD	-20.67 ± 2.58
SS	-23.21 ± 2.24
SSI	8.91 ± 3.55

silicate negatively interferes with the light reception of the solar panel, which may be compensated for using carbon quantum dots. Also, this experiment indicates that an efficiency-improving accessory is feasible. Table 3 shows the means and standard deviations of each of the tested groups, in order to demonstrate the results obtained more clearly. Table 3 shows the average results for each experimental group and the standard deviation associated with those averages. Regarding the gain, we can verify the data presented in Table 4. Based on the data in Table 4, it can be seen that the only experimental group that generated an increase in the generated electrical power was the SSI CQD experimental group. All other experimental groups generated a decrease in the generated electrical power. Regarding the statistical tests applied to the sample results, the normality test results are presented in Table 5.

Table 5. Results of the KS normality tests.

Group	KS Statistics	p-value	Test result
Control	0.06	0.13	Normal
SS CQD	0.05	0.60	Normal
SSI	0.11	0.00	Not normal
SS	0.08	0.02	Not normal
SSI CQD	0.05	0.46	Normal

Table 6. Summary table of the application of the Conover test to the sample groups.

Group	Statistics	p-value
Control vs SS CQD	1.23	0.21
Control vs SSI	-0.42	0.67
Control vs SS	1.14	0.26
Control vs SSI CQD	-4.47	0.00

According to Table 5. the dataset has two groups that do not follow a normal distribution, namely the SSI and SS groups. Therefore, it is not possible to verify whether the samples are statistically distinct using parametric tests (which usually require that the samples follow a normal distribution). For this reason, a non-parametric test (Friedman rank) was applied to evaluate the statistical difference between the samples. Applying the Friedman rank to the sample set generated a statistic of 4481.52 associated with a p-value, $p \approx 0$. Therefore, we can reject the hypothesis that there are no significant differences between the groups. Thus, we can affirm that at least one of the groups is significantly different from the others. To find which groups differ, we applied the Conover test pairwise, generating the data in Table 6. Finally, it can be directly observed from Table 6 that the only experimental group that showed a significant difference in relation to the control group was the SSI CQD group, which is precisely the group that showed the best performance in increasing the generated electrical power.

After 6 months of manufacturing the accessories, all the developed plates showed a visual change, going from translucent to opaque, which negatively interferes with the performance of the solar panel.

4. CONCLUSION

This The treatment on the Si-rich mining residue was effective, increasing Si content from 79.3% (RB) to 92.2% (RT) and reducing Fe from 19.3% to 6.68%. XRD indicated quartz as the main crystalline phase in RT, while the fusion product exhibited characteristic reflections consistent with sodium silicate formation. SEM micrographs further supported the morphological differences between the treated residue and the obtained sodium silicate. Carbon quantum dots were successfully synthesized from chitosan and acetic acid, and FTIR confirmed their formation. Photovoltaic testing showed that the control group presented an average power output of 10.21 ± 0.29 mW, whereas the CQD-doped industrial sodium silicate overlayer (SSI–CQD) achieved 11.12 ± 0.20 mW, corresponding to an 8.9% increase. In contrast, sodium silicate layers without CQDs and residue-derived silicate formulations exhibited lower power outputs than the control. Statistical analysis confirmed that SSI–CQD was the only configuration that increased power generation under the conditions evaluated. After six months, all developed coatings became progressively opaque, indicating limited long-term optical stability and restricting practical implementation. Overall, the results demonstrate the short-term feasibility of an external CQD–silicate overlayer as an accessory for photovoltaic enhancement, while highlighting stability and residue purification as key challenges for future optimization.

ACKNOWLEDGEMENTS

Thanks to the company Inbras for their assistance in the process of separating iron from mining residue.

CREDIT AUTHOR STATEMENT

Camila G. Sastre: Conceptualization, Investigation, Data curation, Writing – original draft. **Juliana de C. Izidoro:** Supervision, Conceptualization, Methodology, Sample characterization, Writing – review & editing. **Wayner de S. Klën:** Supervision, Conceptualization, Writing, Data curation – review & editing. **Mariana Araújo:** Investigation, Sample characterization. **Danilo L. Costa-Silva:** Investigation, Sample characterization.

DECLARATIONS

Conflict of interest The authors declare that they have no known competing financial interests or personal relationships that could have appeared to influence the work reported in this paper.

AVAILABILITY OF DATA

The All data supporting the findings of this study are included within the manuscript. Any additional data related to this work is available from the corresponding author upon reasonable request.

REFERENCES

[1] T.S.C. Bressiani, L. Lorenzini, T.R. Neves, M.B. Alvarenga, S.A.D. Ferreira, P.R.G. Moura, M. de Fátima F. Lelis, Plastic Wood Production from Mining Tailings and Plastic Waste: An Experimental Study, Revista Virtual de Quimica 14 (2022) 372–379. https://doi.org/10.21577/1984-6835.20220080.

[2] J. de Carvalho Izidoro, M.C. Kim, V.F. Bellelli, M.C. Pane, A.B.B. Junior, D.C.R. Espinosa, J.A.S. Tenório, Synthesis of zeolite A using the waste of iron mine tailings dam and its application for industrial effluent treatment, Journal of Sustainable Mining 18 (2019) 277–286. https://doi.org/10.1016/j.jsm.2019.11.001.

[3] Q. M. P. Netto, A.C.R. Guimarães, Caracterização laboratorial de resíduos de mineração como agregado alternativo para misturas asfálticas, Revista Ibero-Americana de Ciências Ambientais 9 (2018) 88–98 http://doi.org/10.6008/CBPC21796858.2018.005.0009.

[4] P. Berardi, J. M. Dias, O mercado da economia circular, GV-EXECUTIVO 17 (2018) 34–37. https://doi.org/10.12660/gvexec.v17n5.2018.77340.

[5] D. G. B. Torres, B.H. de Luca, J. A. Malacarne, J. Souza, D. Casarolli, E. D. C. Silva, T. Guerra, Células fotovoltaicas: desenvolvimento e as três gerações, Revista Técnico-Científica (2019)

[6] C. I. L. Santos, J.C.A. Ferreira, L.R.C. Cunha, R. Vaza, M.A. Schiavona, S\'\intese e caracterização de pontos quânticos ambientalmente amigáveis, um meio simples de exemplificar e explorar aspectos da nanociência e nanotecnologia em cursos de graduação, Quim. Nova 43 (2020) 813–822. https://doi.org/10.21577/0100-4042.20170558.

[7] A. B. F. Vitoreti, L. B. Corrêa, E. Raphael, A. O. T. Patrocinio, A. F. Nogueira, M. A. Schiavon, CÉLULAS SOLARES SENSIBILIZADAS POR PONTOS QUÂNTICOS, Quim. Nova 40 (2017) 436–446. https://doi.org/10.21577/0100-4042.20160192.

[8] O. E. Semonin, J. M. Luther, M. C. Beard, Quantum dots for next-generation photovoltaics, Materials Today 15 (2012) 508–515. https://doi.org/10.1016/S1369-7021(12)70220-1.

[9] S. Rovani, J.J. Santos, P. Corio, D.A. Fungaro, Highly pure silica nanoparticles with high adsorption capacity obtained from sugarcane waste ash, ACS Omega 3 (2018) 2618–2627. https://doi.org/10.1021/acsomega.8b00092.

[10] Gumathannavar R., More R., Lohar A., Kadam M., Shirolkar M.M., Jadhav Y., Koratkar S. DFT-guided photostable chitosan-derived carbon quantum dots as colloidal antibacterial and bioimaging agents. Scientific Reports 16 (2026) 2211. https://doi.org/10.1038/s41598-025-31920-3.

[11] P. R. Bevington, D. K. Robinson, Data reduction and error analysis for the physical sciences, 3rd, ilustrated ed., McGraw-Hill, 2003.

[12] J. R. Taylor, An introduction to error analysis: The study of uncertainties in physical measurements, University Science Books, 1997.

[13] Samuel. Kotz, N. L. Johnson, Breakthroughs in Statistics: Methodology and Distribution, Springer New York, 1992.

[14] Amaral I. B. C., Cavalcante L. C. D., Fabris J. D., Prat B.V., Reis A. B. Use of mining tailings or their sedimentation and flotation fractions in a mixture with soil to produce structural ceramics. Sustainability 13(2) (2021) 911. https://doi.org/10.3390/su13020911.

[15] Zhu D., Pan J., Guo Z., et al. Utilization of high-silicon iron ore tailings for 4N8 high-purity quartz powder production via two-stage acid leaching. Inorganic Chemistry 64(8) (2025) 3805–3823. https://doi.org/10.1021/acs.inorgchem.4c04882.

[16] Ayala-Durán S. C., Hammer P., Nogueira R. F. P. Surface composition and catalytic activity of an iron mining residue for simultaneous degradation of sulfonamide antibiotics. Environmental Science and Pollution Research (2020). https://doi.org/10.1007/s11356-019-06662-1.

[17] Zhan L. T., Ni J. Q., Feng S., Kong L. G., Feng T. Saturated hydraulic conductivity of compacted steel slag-bentonite mixtures: a potential hydraulic barrier material of landfill cover. Waste Management 144 (2022) 349–356. https://doi.org/10.1016/j.wasman.2022.04.004.

[18] Li Y., Li S., Zhao X., Pan X., Guo P. Separation and purification of high-purity quartz from high-silicon iron ore tailing: An innovative strategy for comprehensive utilization of tailings resources. Process Safety and Environmental Protection 169 (2023) 142–148. https://doi.org/10.1016/j.psep.2022.11.006.

[19] B. A. Dedavid, C. I. Gomes, G. Machado, Microscopia eletrônica de varredura: aplicações e preparação de amostras: materiais poliméricos, metálicos e semicondutores, EdiPUCRS, 2007.

[20] X. Liu, J. Pang, F. Xu, X. Zhang, Simple approach to synthesize amino-functionalized carbon dots by carbonization of chitosan, Sci. Rep. 6 (2016) 31100. https://doi.org/10.1038/srep31100.

[21] A. Konwar, N. Gogoi, G. Majumdar, D. Chowdhury, Green chitosan–carbon dots nanocomposite hydrogel film with superior properties, Carbohydr. Polym. 115 (2015) 238–245. https://doi.org/10.1016/j.carbpol.2014.08.021.